To be published in Optics Letters:

Title: Monolithically integrated photonic crystal surface emitters on silicon with vortex beam by using bound states in the continuum

Authors: Haochuan Li,Mingchu Tang,Taojie Zhou,Wentao xie,Renjie Li,Yuanhao Gong,MICKAEL MARTIN,THIERRY BARON,Siming Chen,Huiyun Liu,Zhaoyu Zhang

Accepted: 20 February 23

Posted 21 February 23

DOI: https://doi.org/10.1364/OL.484472

Monolithically integrated photonic crystal surface emitters on silicon with vortex beam by using bound states in the continuum

Haochuan Li,[1,†] Mingchu Tang,[3,†] Taojie Zhou,[1,3] Wentao Xie,[1] Renjie Li,[1,2] Yuanhao Gong,[1] Mickael Martin, [4] Thierry Baron, [4] Siming Chen,[3, a)] Huiyun Liu,[3, a)] Zhaoyu Zhang[1, a)]

[1]*Guangdong Key Laboratory of Optoelectronic Materials and Chips and Shenzhen Key Lab of Semiconductor Lasers, School of Science and Engineering, The Chinese University of Hong Kong, Shenzhen, 518172, PR China*

[2]*Shenzhen Research Institute of Big Data, Shenzhen, Guangdong, 518172, PR China*

[3]*Department of Electronic and Electrical Engineering, University College London, London, Torrington Place, WC1E 7JE, UK*

[4]*Univ. Grenoble Alpes, CNRS, CEA-LETI, MINATEC, LTM, F-38054 Grenoble, France*

[†]*These authors contributed equally to this work.*

[a)] *Authors to whom correspondence should be addressed: siming.chen@ucl.ac.uk, huiyun.liu@ucl.ac.uk, zhangzy@cuhk.edu.cn*

Optical resonant cavities with high quality factor (Q-factor) are widely used in science and technology for their capability of strong confinement of light and enhanced light-matter interaction. The 2D photonic crystal structure with bound states in the continuum (BICs) is a novel concept for resonators with ultra-compact device size, which can be used to generate surface emitting vortex beams based on symmetry-protected BICs at the Γ point. Here, to the best of our knowledge, we demonstrate the first photonic crystal surface emitter with vortex beam by using BICs monolithically grown on CMOS-compatible silicon substrate. The fabricated quantum-dot BICs-based surface emitter operates at 1.3 μm under room temperature (RT) with a low continuous wave (CW) optically pumped condition. We also reveal the BIC's amplified spontaneous emission with the property of polarization vortex beam, which is promising to provide novel degree of freedom in classical and quantum realms.

In recent decades, great attention has been paid to finding promising light sources that own the merits of both ultralow energy consumption and small footprint to realize the goal of on-chip integrated optoelectronics [1, 2]. It is usually problematic to pursue a large Purcell factor (proportional to Q/V_{mode}) while keeping a high output power in micro resonators such as the whispering-gallery-mode based micro-disk lasers and photonic crystal (PhC) defect cavity lasers [3-7]. Particularly, on-chip integrated and ultra-compact vortex emitters by employing BICs can naturally generate vortex beams with high quality factor (Q-factor) [8-12]. Since the first demonstration of BIC, numerous schemes to design BIC modes have been proposed, including C_2^z-symmetry protected BIC [13, 14], resonance-trapped BIC based on Mie resonance [15, 16], electromagnetically induced transparency (EIT) based on quasi-BIC [17, 18], mini-BICs [19], quasi-BICs [20], and multimode laser based on two non-degenerate BIC modes [21]. Symmetry-protected BIC resonators present extra benefits of vector beam emission which render them suitable for the on-chip integration and next-generation smart production and mobility.

Meanwhile, the realization of monolithic integration of high-performance III-V semiconductor light sources on CMOS-compatible silicon platform is of great importance to promote the next-generation Si-based on-chip light emitters for a high-yield and scalability in real production scenarios [22]. Resonant-cavity light-emitting diode (RCLED) is an appealing candidate of short-distance communication systems for its narrow spectral linewidth, narrow divergence, high luminous intensity, and energy efficiency [23, 24]. However, so far, light sources with surface emitting beams based on BICs monolithically grown on silicon have not been demonstrated.

Here, we demonstrate a room temperature (RT) μW-level continuous wave (CW) optically pumped PhC surface emitter with vortex beam monolithically grown on Si based on symmetry-protected BICs with the potential of on-chip integrated RCLED and BIC lasers. Symmetry-protected BIC resonators present extra benefits of vector beam emission, which render them suitable for the on-chip integration and next-generation smart production and mobility. In addition, optical vortex emitters with a helical wavefront and associated orbital angular momentum (OAM) are at the heart of wide-range potential applications, including free-space

communications, high-resolution optical microscopy, and quantum communications [25].

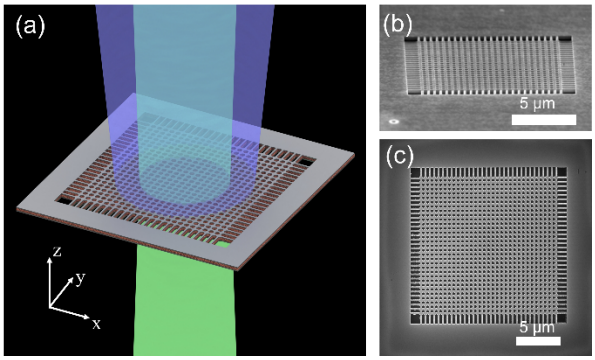

Fig. 1. (a) Schematic of the designed BIC emitter monolithically grown on silicon. The device is schematically pumped by focused purple laser light, producing a green vortex beam. (b), (c) Scanning electron microscopy images of InAs QDs BIC emitter suspended in air.

The designed BIC emitters are illustrated in Fig. 1(a). Fig. 1(b) and 1(c) show the tilted and top-view scanning electron microscopy (SEM) images of fabricated device, respectively. The detailed wafer information and epitaxial layer structure is described in the supplementary material.

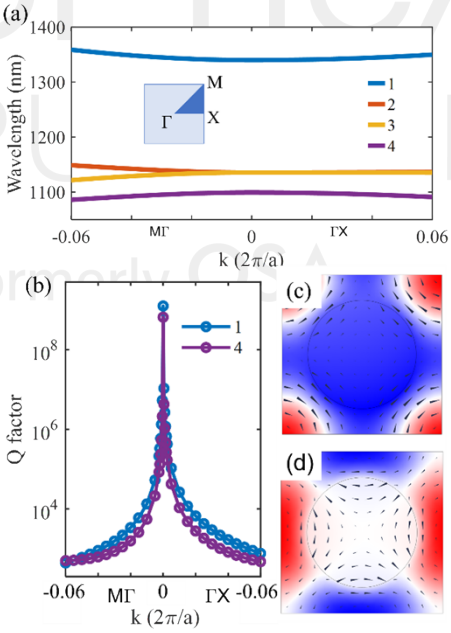

Fig. 2. (a) Dispersion relation of designed BIC structure for TE modes in both MΓ and ΓX directions. Modes 1 to 4 denote four resonant modes at Γ point for four energy bands, respectively. The inset shows the first Brillouin zone. Calculated *Q*-factors of resonant mode 1 and mode 4 are shown in (b). Mode 1 and 4 are symmetry-protected BIC modes with a high-*Q* factor at Γ point. (c) and (d) shows the simulated H_z field distribution in a unit cell of mode 1 and 4, respectively. The arrows present the in-plane electric field direction.

To attain the designed BICs structure, we first deposited a layer of SiO_2 with a thickness of ~ 200 nm on the as-grown wafer by plasma-enhanced chemical vapor deposition as a hard mask. Then, 200 nm ZEP520A electron beam resist was spin-coated on the surface of the hard mask. The PhC pattern was created by electron beam lithography (EBL) and subsequently transferred to the hard mask, the active layer, and the sacrificial layer by inductively coupled plasma reactive ion etching. Finally, the fabricated sample was suspended in the air by immersing devices in 40% hydrofluoric acid solution for 30 seconds. The sacrificial layer $Al_{0.6}Ga_{0.4}As$ with a thickness of 1 μm was removed to form a hollow region under the emitter to enhance the light confinement in vertical direction.

The designed structure was simulated by using a three-dimensional eigenfrequency solver in COMSOL Multiphysics. The structural parameters in the simulation model are radius of air holes r = 170 nm, lattice constant a = 500 nm, thickness of the slab T = 362 nm, and the refractive index n = 3.4. Fig. 2(a) shows the dispersion relation of BIC structure for TE-like modes along ΓX directions, where M, Γ, X are high-symmetry points of the reduced Brillouin zone for a square PhC structure. The calculated *Q*-factors of these modes are described in Fig. 2(b), where we can find

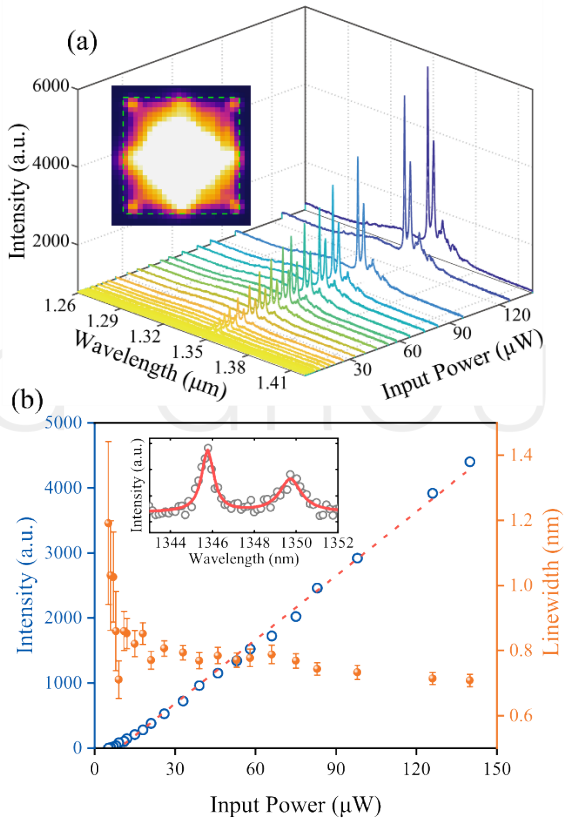

Fig. 3. (a) Evolution of the emission spectrum as the function of the input powers. The inset presents a near-field mode pattern image measured by using an infrared camera. The boundary of the emitter is also indicated by the dash line. (b) shows the output intensity as a function of the input powers for the peak of ~ 1345.8 nm. The inset shows the emission spectrum measured at low input power and the corresponding Lorentzian curve fitting.

two high *Q*-factor symmetry-protected BIC modes (mode 1 and mode 4) at Γ point. The calculated H_z field profiles of mode 1 and mode 4 with vorticity of field distribution are plotted in the Fig. 2(c) and Fig. 2(d), respectively. We can deduce that these high-*Q* modes are even modes with 180° rotational symmetry (C_2) around the *z*-axis (mode 1 has C_4 rotational symmetry), which corresponds with

the features of BIC modes and implies the emission behavior as a vector beam with azimuthal polarization[10]. The symmetry-protected BIC modes are decoupled from radiation continuum owing to symmetry mismatch at Γ point, thus yielding a strong local confinement. The *Q*-factor drops rapidly off Γ point, which illustrates the high demand for the symmetry of the structure to form the symmetry-protected BIC modes.

The fabricated emitter was optically pumped at RT by using a CW 632.8 nm He-Ne laser. The measured spectra under various pumping powers of the designed emitter with a = 510 nm and r = 170 nm are shown in Fig. 3(a). Single mode emission is expected to be achieved of fabricated devices with the high *Q*-factor resonant mode (mode 1 in Fig. 2), due to that only the mode 1 at Γ point is within the ground state emission region of grown QDs under low excitation pump powers. However, there are slight discrepancies between the simulated and experimental results. Two resonant peaks at around 1345.8 nm and 1349.8 nm are simultaneously observed.

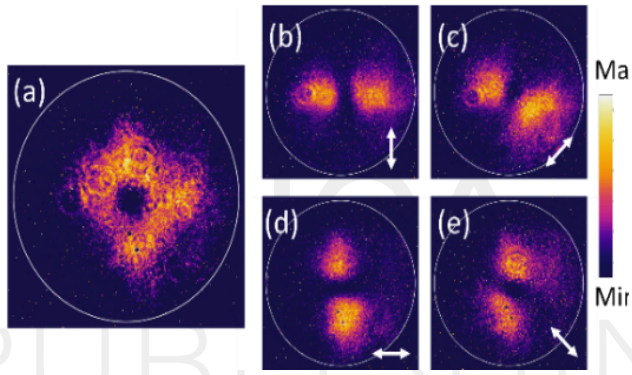

Fig. 4. (a) The far-field intensity distribution of the vortex beam exhibits a doughnut-shaped profile, which verifies the emission from BIC modes. (b)-(e) represent the measured polarization-resolved images of the vortex beam by placing a linear polarizer in front of the infrared camera.

The collected intensity (L–L) and the linewidth of the spectrum peak under various pumping powers are shown in Fig. 3(b). A decrease of linewidth can be observed from the L-L curve, which indicates the existence of amplified spontaneous emission. The inset in Fig. 3(b) shows the Lorentzian curve fitting of collected data at low input power.

The *Q*-factor of the system can be estimated by using $Q = \lambda/\Delta\lambda$, where the λ is the central wavelength of the resonant peak, and the Δλ is the linewidth of the resonant peak. The experimental *Q*-factor of this device was calculated as around 1.9×10^3 . This is much lower than the theoretically simulated results, which can be explained by the fact that BICs with infinite *Q*-factor and zero leakage are obtained only for infinitely extended structures. However, the experimentally fabricated-devices have finite periods of PhCs, leading to a large radiation loss in the system and the BIC become leaky with finite *Q*-factor [10,26]. We also pay attention to the two resonant peaks emerging in the emission spectrum, which can be explained by the imperfection of the device fabrication, which might break the symmetry of fabricated devices. The imperfection can originate from the etching profiles, nonuniform thickness of epitaxial layer and the position of the PhC air holes. Since the symmetry-protected BIC modes are highly sensitive to symmetry breaking, the imperfection may diffract BIC modes into radiation channels, thus bringing another exceptional leaky resonant peak and increasing radiation loss. The nonuniform polarization distribution of far-field beam profile also indicates the imperfection. To further enhance robustness to fabrication imperfection, reduce out-of-plane losses and achieve ultralow lasing threshold BIC lasers, super-BIC mode can be utilized, which is created by merging symmetry-protected and accidental BICs in the momentum space [27].

To further demonstrate the vortex characteristics of BIC emitters, the method of back focal plane imaging [9] was implemented to study the far-field angular distributions of BIC modes. The spatially distributed intensity appears as the shape of a doughnut with a dark zone at the center as shown in Fig. 4(a). The central dark core is due to the topological singularity at the center of the BIC structure. The polarization-resolved images were further measured, which presents two lobes vertical to the direction of polarization and confirms the azimuthal polarization of the emission light of BIC mode as depicted in Figs. 4(b)-(e).

Table 1. Comparison of this work with other state-of-art BIC lasers in the literature. Short hyphens mean no data available or produced.

Reference	BIC Type	Gain material	Threshold peak pumping power (mW)	*Q*-factor	FWHM	Monolithically grown on Si	CW pumping
This work	Symmetry-protected BIC	InAs/GaAs DWELL	-	1.9×10^3	0.71nm	Yes	**Yes**
Wang 2021 [28]	Symmetry-protected BIC	PVK	-	1.2×10^3	0.59nm	No	No
Hwang 2021 [27]	Super BIC	InGaAsP MQWs	0.34	7.3×10^3	0.22nm	No	No
Wu 2021 [15]	Symmetry-protected BIC	PVK QDs	-	-	-	No	No
Huang 2020 [10]	Symmetry-protected BIC	PVK	5.28×10^5	-	-	No	No
Ge 2019 [29]	Symmetry-protected BIC	Monolayer WS_2	-	2.5×10^3	0.25nm	No	Yes
Ha 2018 [30]	Symmetry-protected BIC	GaAs	8.8×10^5	2.75×10^3	0.3nm	No	No
Kodigala 2017 [8]	Symmetry-protected BIC	InGaAsP MQWs	15.6	4.7×10^3	0.33nm	No	No
Yu 2021 [31]	Fano BIC	InGaAsP SQW	3.5	7.8×10^4	0.02nm	No	Yes
Wu 2020 [15]	Symmetry-protected BIC	CdSe	5.09×10^8	2.59×10^3	0.25nm	No	No
Mohamed 2020 [21]	Symmetry-protected BIC	IR-792 molecules	2.16×10^6	2.88×10^3	0.30nm	No	No

Although the emitter does not exhibit clear lasing behavior, as the first BIC emitter monolithically grown on Si, the device maintains the FWHM under 0.8nm while the CW pumping power is as low as 60 μW. The key performance of the BIC emitter demonstrated in this work is also compared with other state-of-art BIC lasers in the literature, as shown in Table 1. In general, our emitter shows a comparable *Q*-factor under CW pumping condition to other symmetry-protected BIC lasers. But owing to a shortage of pulsed pumping equipment in our lab, we failed to conduct further pulse-pumped experiments for potential lasing phenomenon. This issue could be resolved in future by collaboration and by improvement in fabrication.

In conclusion, we present the PhC surface emitter monolithically integrated on silicon substrate by using BICs with vortex beam. The emitter was CW optically pumped at RT and the properties of BIC modes were analyzed with numerical simulations and we verified the vorticity of the BIC vortex beam experimentally. The promising emission characteristics of the emitter based on BICs with an ultralow input power, vertical emission direction, and vortex beam monolithically grown on Si (001) substrate provide more possibilities of application for on-chip ultra-compact BIC lasers and large-scale integration of optoelectronic devices on a silicon platform.

Funding

This work was supported by National Natural Science Foundation of China (62174144), Shenzhen Science and Technology Program (JCYJ20210324115605016, JCYJ20210324120204011, JSGG20210802153540017, JCYJ20220818102214030), Shenzhen Key Laboratory Project (ZDSYS201603311644527), Guangdong Key Laboratory of Optoelectronic Materials and Chips (2022KSYS014) , Optical Communication Core Chip Research Platform, Shenzhen Research Institute of Big Data, UK Engineering and Physical Sciences Research Council (EP/P006973/1, EP/T01394X/1, EP/T028475/1), National Epitaxy Facility, European project H2020-ICT-PICTURE (780930), Royal Academy of Engineering (RF201617/16/28), French National Research Agency under the Investissements d'avenir ANR-10-IRT-05 and ANR-15-IDEX-02 and French RENATECH network. The devices were manufactured in Core Research Facilities (CRF) at SUSTech, and the authors would like to thank the engineers for their technical support. Helpful discussions with Jingwen Ma are also acknowledged. S. C. thanks the Royal Academy of Engineering for funding his Research Fellowship.

Disclosures

The authors declare no conflict of interest.

Supplementary Material

The supplementary material can be found in the journal repository.

References

1. C. Sun, M. T. Wade, Y. Lee, J. S. Orcutt, L. Alloatti, M. S. Georgas, A. S. Waterman, J. M. Shainline, R. R. Avizienis, S. Lin, B. R. Moss, R. Kumar, F. Pavanello, A. H. Atabaki, H. M. Cook, A. J. Ou, J. C. Leu, Y. H. Chen, K. Asanovic, R. J. Ram, M. A. Popovic, and V. M. Stojanovic, Nature **528** (7583), 534 (2015).
2. T. Komljenovic, D. Huang, P. Pintus, M. A. Tran, M. L. Davenport, and J. E. Bowers, Proceedings of the IEEE **106**, 2246 (2018).
3. H. Altug, D. Englund, and J. Vučković, Nature Phys **2**, 484 (2006).
4. O. Painter, R. K. Lee, A. Scherer, A. Yariv, J. D. O'Brien, P. D. Dapkus, and I. Kim, Science **284**, 1819 (1999).
5. K. Nozaki, A. Shinya, S. Matsuo, Y. Suzaki, T. Segawa, T. Sato, Y. Kawaguchi, R. Takahashi, and M. Notomi, Nature Photon **6**, 248–252 (2012).
6. T. Zhou, J. Zhou, Y. Cui, X. Liu, J. Li, K. He, X. Fang, and Z. Zhang, Opt. Express, OE **26**, 16797–16804 (2018).
7. T. Zhou, K. W. Ng, X. Sun, and Z. Zhang, Nanophotonics **9**, 2997–3002 (2020).
8. A. Kodigala, T. Lepetit, Q. Gu, B. Bahari, Y. Fainman, and B. Kanté, Nature **541**, 196–199 (2017).
9. S. I. Azzam and A. V. Kildishev, Adv. Optical Mater. **9**, 2001469 (2021).
10. C. Huang, C. Zhang, S. Xiao, Y. Wang, Y. Fan, Y. Liu, N. Zhang, G. Qu, H. Ji, J. Han, L. Ge, Y. Kivshar, and Q. Song, Science **367**, 1018 (2020).
11. C. W. Hsu, B. Zhen, A. D. Stone, J. D. Joannopoulos, and M. Soljačić, Nat Rev Mater **1**, 16048 (2016).
12. B. Zhen, C. W. Hsu, L. Lu, A. D. Stone, and M. Soljacic, Phys Rev Lett **113** (25), 257401 (2014).
13. S. A. Dyakov, M. V. Stepikhova, A. A. Bogdanov, A. V. Novikov, D. V. Yurasov, M. V. Shaleev, Z. F. Krasilnik, S. G. Tikhodeev, and N. A. Gippius, Laser & Photonics Reviews 15, 2000242 (2021).
14. J. F. Algorri, F. Dell'Olio, P. Roldán-Varona, L. Rodríguez-Cobo, J. M. López-Higuera, J. M. Sánchez-Pena, and D. C. Zografopoulos, Opt. Express, OE **29**, 10374 (2021).
15. M. Wu, S. T. Ha, S. Shendre, E. G. Durmusoglu, W.-K. Koh, D. R. Abujetas, J. A. Sánchez-Gil, R. Paniagua-Domínguez, H. V. Demir, and A. I. Kuznetsov, Nano Lett. 20, 6005–6011 (2020).
16. I.-C. Benea-Chelmus, S. Mason, M. L. Meretska, D. L. Elder, D. Kazakov, A. Shams-Ansari, L. R. Dalton, and F. Capasso, Nat Commun 13, 1–9 (2022).
17. J. F. Algorri, F. Dell'Olio, P. Roldán-Varona, L. Rodríguez-Cobo, J. M. López-Higuera, J. M. Sánchez-Pena, V. Dmitriev, and D. C. Zografopoulos, Opt. Express, OE 30, 4615–4630 (2022).
18. D. R. Abujetas, Á. Barreda, F. Moreno, A. Litman, J.-M. Geffrin, and J. A. Sánchez-Gil, Laser & Photonics Reviews 15, 2000263 (2021).
19. Z. Chen, X. Yin, J. Jin, Z. Zheng, Z. Zhang, F. Wang, L. He, B. Zhen, and C. Peng, Science Bulletin 67, 359–366 (2022).
20. Z. Liu, Y. Xu, Y. Lin, J. Xiang, T. Feng, Q. Cao, J. Li, S. Lan, and J. Liu, Phys. Rev. Lett. 123, 253901 (2019).
21. S. Mohamed, J. Wang, H. Rekola, J. Heikkinen, B. Asamoah, L. Shi, and T. K. Hakala, Laser & Photonics Reviews 16, 2100574 (2022).
22. D. Thomson, A. Zilkie, J. E. Bowers, T. Komljenovic, G. T. Reed, L. Vivien, D. Marris-Morini, E. Cassan, L. Virot, J.-M. Fédéli, J.-M. Hartmann, J. H. Schmid, D.-X. Xu, F. Boeuf, P. O'Brien, G. Z. Mashanovich, and M. Nedeljkovic, J. Opt. **18**, 073003 (2016).
23. E. F. Schubert, Light-emitting diodes (E. Fred Schubert, 2018).
24. E. F. Schubert, N. E. J. Hunt, M. Micovic, R. J. Malik, D. L. Sivco, A. Y. Cho, and G. J. Zydzik, Science **265**, 943 (1994).
25. P. Miao, Z. Zhang, J. Sun, W. Walasik, S. Longhi, N. M. Litchinitser, and L. Feng, Science **353**, 464 (2016).
26. M. Minkov, D. Gerace, and S. Fan, Optica, OPTICA **6**, 1039–1045 (2019).
27. M.-S. Hwang, H.-C. Lee, K.-H. Kim, K.-Y. Jeong, S.-H. Kwon, K. Koshelev, Y. Kivshar, and H.-G. Park, Nat Commun **12**, 4135 (2021).
28. Y. Wang, Y. Fan, X. Zhang, H. Tang, Q. Song, J. Han, and S. Xiao, ACS Nano (2021).
29. X. Ge, M. Minkov, S. Fan, X. Li, and W. Zhou, npj 2D Mater Appl 3, 16 (2019).
30. S. T. Ha, Y. H. Fu, N. K. Emani, Z. Pan, R. M. Bakker, R. Paniagua-Domínguez, and A. I. Kuznetsov, Nature Nanotech 13, 1042 (2018).
31. Y. Yu, A. Sakanas, A. R. Zali, E. Semenova, K. Yvind, and J. Mørk, Nat. Photon. 15, 758 (2021).

FULL REFERENCES

1. C. Sun, M. T. Wade, Y. Lee, J. S. Orcutt, L. Alloatti, M. S. Georgas, A. S. Waterman, J. M. Shainline, R. R. Avizienis, S. Lin, B. R. Moss, R. Kumar, F. Pavanello, A. H. Atabaki, H. M. Cook, A. J. Ou, J. C. Leu, Y. H. Chen, K. Asanovic, R. J. Ram, M. A. Popovic, and V. M. Stojanovic, "Single-chip microprocessor that communicates directly using light," Nature **528**, 534–8 (2015).
2. T. Komljenovic, D. Huang, P. Pintus, M. A. Tran, M. L. Davenport, and J. E. Bowers, "Photonic integrated circuits using heterogeneous integration on silicon," Proc. IEEE **106**, 2246–2257 (2018).
3. H.Altug, D.Englund, and J.Vuc̆ković,"Ultrafast photonic crystal nanocavity laser," Nat. Phys. **2**, 484–488 (2006).
4. O. Painter, R. K. Lee, A. Scherer, A. Yariv, J. D. O'Brien, P. D. Dapkus, and I. I. Kim, "Two-dimensional photonic band-gap defect mode laser," Science **284**, 1819–21 (1999).
5. K. Nozaki, A. Shinya, S. Matsuo, Y. Suzaki, T. Segawa, T. Sato, Y. Kawaguchi, R. Takahashi, and M. Notomi, "Ultralow-power all-optical RAM based on nanocavities," Nature Photon **6**, 248–252 (2012).
6. T. Zhou, J. Zhou, Y. Cui, X. Liu, J. Li, K. He, X. Fang, and Z. Zhang, "Microscale local strain gauges based on visible micro-disk lasers embedded in a flexible substrate," Opt. Express, OE **26**, 16797–16804 (2018).
7. T. Zhou, K. W. Ng, X. Sun, and Z. Zhang, "Ultra-thin curved visible microdisk lasers with three-dimensional whispering gallery modes," Nanophotonics **9**, 2997–3002 (2020).
8. A. Kodigala, T. Lepetit, Q. Gu, B. Bahari, Y. Fainman, and B. Kanté, "Lasing action from photonic bound states in continuum," Nature **541**, 196–199 (2017).
9. S. I. Azzam and A. V. Kildishev, "Photonic Bound States in the Continuum: From Basics to Applications," Adv. Optical Mater. **9**, 2001469 (2021).
10. C. Huang, C. Zhang, S. Xiao, Y. Wang, Y. Fan, Y. Liu, N. Zhang, G. Qu, H. Ji, J. Han, L. Ge, Y. Kivshar, and Q. Song, "Ultrafast control of vortex microlasers," Science **367**, 1018–1021 (2020).
11. C. W. Hsu, B. Zhen, A. D. Stone, J. D. Joannopoulos, and M. Soljačić, "Bound states in the continuum," Nat Rev Mater **1**, 16048 (2016).
12. B. Zhen, C. W. Hsu, L. Lu, A. D. Stone, and M. Soljačić, "Topological Nature of Optical Bound States in the Continuum," Phys. Rev. Lett. **113**, 257401 (2014).
13. S. A. Dyakov, M. V. Stepikhova, A. A. Bogdanov, A. V. Novikov, D. V. Yurasov, M. V. Shaleev, Z. F. Krasilnik, S. G. Tikhodeev, and N. A. Gippius, "Photonic Bound States in the Continuum in Si Structures with the Self-Assembled Ge Nanoislands," Laser & Photonics Reviews **15**, 2000242 (2021).
14. J. F. Algorri, F. Dell'Olio, P. Roldán-Varona, L. Rodríguez-Cobo, J. M. López-Higuera, J. M. Sánchez-Pena, and D. C. Zografopoulos, "Strongly resonant silicon slot metasurfaces with symmetry-protected bound states in the continuum," Opt. Express, OE **29**, 10374–10385 (2021).
15. M. Wu, S. T. Ha, S. Shendre, E. G. Durmusoglu, W.-K. Koh, D. R. Abujetas, J. A. Sánchez-Gil, R. Paniagua-Domínguez, H. V. Demir, and A. I. Kuznetsov, "Room-Temperature Lasing in Colloidal Nanoplatelets via Mie-Resonant Bound States in the Continuum," Nano Lett. **20**, 6005–6011 (2020).
16. I.-C. Benea-Chelmus, S. Mason, M. L. Meretska, D. L. Elder, D. Kazakov, A. Shams-Ansari, L. R. Dalton, and F. Capasso, "Gigahertz free-space electro-optic modulators based on Mie resonances," Nat Commun 13, 1–9 (2022).
17. J. F. Algorri, F. Dell'Olio, P. Roldán-Varona, L. Rodríguez-Cobo, J. M. López-Higuera, J. M. Sánchez-Pena, V. Dmitriev, and D. C. Zografopoulos, "Analogue of electromagnetically induced transparency in square slotted silicon metasurfaces supporting bound states in the continuum," Opt. Express, OE **30**, 4615–4630 (2022).
18. D. R. Abujetas, Á. Barreda, F. Moreno, A. Litman, J.-M. Geffrin, and J. A. Sánchez-Gil, "High-Q Transparency Band in All-Dielectric Metasurfaces Induced by a Quasi Bound State in the Continuum," Laser & Photonics Reviews 15, 2000263 (2021).
19. Z. Chen, X. Yin, J. Jin, Z. Zheng, Z. Zhang, F. Wang, L. He, B. Zhen, and C. Peng, "Observation of miniaturized bound states in the continuum with ultra-high quality factors," Science Bulletin **67**, 359–366 (2022).
20. Z. Liu, Y. Xu, Y. Lin, J. Xiang, T. Feng, Q. Cao, J. Li, S. Lan, and J. Liu, "High- Q Quasibound States in the Continuum for Nonlinear Metasurfaces," Phys. Rev. Lett. **123**, 253901 (2019).
21. S. Mohamed, J. Wang, H. Rekola, J. Heikkinen, B. Asamoah, L. Shi, and T. K. Hakala, "Controlling Topology and Polarization State of Lasing Photonic Bound States in Continuum," Laser & Photonics Reviews **16**, 2100574 (2022).
22. D. Thomson, A. Zilkie, J. E. Bowers, T. Komljenovic, G. T. Reed, L. Vivien, D. Marris-Morini, E. Cassan, L. Virot, J.-M. Fédéli, J.-M. Hartmann, J. H. Schmid, D.-X. Xu, F. Boeuf, P. O'Brien, G. Z. Mashanovich, and M. Nedeljkovic, "Roadmap on silicon photonics," J. Opt. **18**, 073003 (2016).
23. E. F. Schubert, Light-emitting diodes (E. Fred Schubert, 2018).
24. E. F. Schubert, N. E. J. Hunt, M. Micovic, R. J. Malik, D. L. Sivco, A. Y. Cho, and G. J. Zydzik, "Highly Efficient Light-Emitting Diodes with Microcavities," Science **265**, 943–945 (1994).
25. P. Miao, Z. Zhang, J. Sun, W. Walasik, S. Longhi, N. M. Litchinitser, and L. Feng, "Orbital angular momentum microlaser," Science **353**, 464–467 (2016).
26. M. Minkov, D. Gerace, and S. Fan, "Doubly resonant $\chi^{(2)}$ nonlinear photonic crystal cavity based on a bound state in the continuum," Optica, OPTICA **6**, 1039–1045 (2019).
27. M.-S. Hwang, H.-C. Lee, K.-H. Kim, K.-Y. Jeong, S.-H. Kwon, K. Koshelev, Y. Kivshar, and H.-G. Park, "Ultralow-threshold laser using super-bound states in the continuum," Nat Commun **12**, 4135 (2021).
28. Y. Wang, Y. Fan, X. Zhang, H. Tang, Q. Song, J. Han, and S. Xiao, "Highly Controllable Etchless Perovskite Microlasers Based on Bound States in the Continuum," ACS Nano **15**, 7386–7391 (2021).
29. X. Ge, M. Minkov, S. Fan, X. Li, and W. Zhou, "Laterally confined photonic crystal surface emitting laser incorporating monolayer tungsten disulfide," npj 2D Mater Appl **3**, 1–5 (2019).
30. S. T. Ha, Y. H. Fu, N. K. Emani, Z. Pan, R. M. Bakker, R. Paniagua-Domínguez, and A. I. Kuznetsov, "Directional lasing in resonant semiconductor nanoantenna arrays," Nature Nanotech **13**, 1042–1047 (2018).
31. Y. Yu, A. Sakanas, A. R. Zali, E. Semenova, K. Yvind, and J. Mørk, "Ultra-coherent Fano laser based on a bound state in the continuum," Nat. Photon. **15**, 758–764 (2021).